General Disclaimer

One or more of the Following Statements may affect this Document

- This document has been reproduced from the best copy furnished by the organizational source. It is being released in the interest of making available as much information as possible.

- This document may contain data, which exceeds the sheet parameters. It was furnished in this condition by the organizational source and is the best copy available.

- This document may contain tone-on-tone or color graphs, charts and/or pictures, which have been reproduced in black and white.

- This document is paginated as submitted by the original source.

- Portions of this document are not fully legible due to the historical nature of some of the material. However, it is the best reproduction available from the original submission.

NASA TM X- 73,115

A SUBMERGED SINGULARITY METHOD FOR CALCULATING POTENTIAL FLOW VELOCITIES AT ARBITRARY NEAR-FIELD POINTS

Brian Maskew

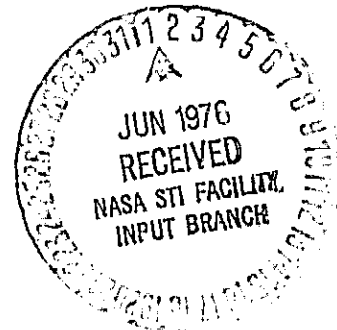Ames Research Center
Moffett Field, Calif. 94035

March 1976

1. Report No. TM X-73,115	2. Government Accession No.	3. Recipient's Catalog No.
4. Title and Subtitle A SUBMERGED SINGULARITY METHOD FOR CALCULATING POTENTIAL FLOW VELOCITIES AT ARBITRARY NEAR-FIELD POINTS		5. Report Date
		6. Performing Organization Code
7. Author(s) Brian Maskew		8. Performing Organization Report No. A-6498
9. Performing Organization Name and Address NASA Ames Research Center Moffett Field, Calif. 94035		10. Work Unit No. 505-06-11
		11. Contract or Grant No.
12. Sponsoring Agency Name and Address National Aeronautics and Space Administration Washington, D.C. 20546		13. Type of Report and Period Covered Technical Memorandum
		14. Sponsoring Agency Code

15. Supplementary Notes

16. Abstract

A discrete singularity method has been developed for calculating the potential flow around two-dimensional airfoils. The objective was to calculate velocities at any *arbitrary* point in the flow field, including points that approach the airfoil surface. That objective was achieved and is demonstrated here on a Joukowski airfoil. The method used combined vortices and sources "submerged" a small distance below the airfoil surface and incorporated a near-field subvortex technique developed earlier. When a velocity calculation point approached the airfoil surface, the number of discrete singularities effectively increased (but only locally) to keep the point just outside the error region of the submerged singularity discretization. The method could be extended to three dimensions, and should improve nonlinear methods, which calculate interference effects between multiple wings, and which include the effects of force-free trailing vortex sheets. The capability demonstrated here would extend the scope of such calculations to allow the close approach of wings and vortex sheets (or vortices).

17. Key Words (Suggested by Author(s)) Aircraft aerodynamics Subsonic flow Potential flow	18. Distribution Statement Unlimited STAR Category - 02
19. Security Classif. (of this report) Unclassified	20. Security Classif. (of this page) Unclassified	21. No. of Pages 26	22. Price* $3.75

Table of Contents

A Submerged Singularity Method for Calculating
Potential Flow Velocities at Arbitrary Near-Field Points

Brian Maskew*

Ames Research Center, NASA, Moffett Field, California 94035

Summary

A discrete singularity method has been developed for calculating the potential flow around two-dimensional airfoils. The objective was to calculate velocities at any *arbitrary* point in the flow field, including points that approach the airfoil surface. That objective was achieved and is demonstrated here on a Joukowski airfoil. The method used combined vortices and sources "submerged" a small distance below the airfoil surface and incorporated a near-field subvortex technique developed earlier. When a velocity calculation point approached the airfoil surface, the number of discrete singularities effectively increased (but only locally) to keep the point just outside the error region of the submerged singularity discretization. The method could be extended to three dimensions and should improve nonlinear methods, which calculate interference effects between multiple wings, and which include the effects of force-free trailing vortex sheets. The capability demonstrated here would extend the scope of such calculations to allow the close approach of wings and vortex sheets (or vortices).

Nomenclature

Δ = length of vortex sheet represented by a discrete vortex (approximately equal to the distance between the two control points adjacent to the vortex)

ΔS_k = distance along the vortex sheet between the kth and the $k + 1$ th basic vortices (Eq. (5))

θ = angle parameter for positioning the vortices, Eq. (3)

$\Delta\theta$ = increment in θ between two basic vortices

$\delta\theta$ = increment in θ between two subvortices

S = surface length (Eq. (3))

s_v = surface length measured to a basic vortex from the beginning of a region (i.e., from $\theta = 0$)

$\underline{R}$ = position vector for basic vortices

$\underline{r}$ = position vector for subvortices

$\underline{a}$ = position vector of a calculation point relative to a vortex

a = modulus of $\underline{a}$, etc.

$\underline{n}$ = unit normal vector at the airfoil surface

$\underline{i},\underline{k}$ = cartesian unit vector system (Fig. 1)

H = height of a velocity calculation point above the local vortex sheet

$\underline{V}$ = velocity vector

$\left.\begin{matrix} U \\ W \end{matrix}\right\}$ = components of the vortex-induced velocity vector in the $\underline{i}$ and $\underline{k}$ directions, respectively (Fig. 1)

Γ = vortex strength

D = piecewise-constant doublet strength, i.e., strength of opposing vortices at each end of a doublet panel (Fig. 3)

2

σ = source strength

C_L = lift coefficient

C_D = drag coefficient

C_M = pitching moment coefficient about the origin

NBS = number of basic singularities

NSV = number of subvortices used on a segment between two basic vortices

FNS = factor on the number of subvortices (Eq. (1))

NRF = near-field radius factor, applied to Δ (Subsection 3.3)

SDF = submerged depth factor, applied to Δ

SSF = subvortex strength factor (Eq. (4))

1.0 Introduction

This is the second paper from a work program aimed at removing the close-approach problem associated with vortex-lattice methods. The first paper[1] described a subvortex technique by which the near-field problem area of a discretized vortex sheet could be reduced to a small region, and showed an application in a free-vortex sheet rollup calculation. The present paper is concerned with potential flow pressure calculations at arbitrary surface points on thick, two-dimensional airfoils.

The objective of this study was to predict the velocity at any arbitrary point in the flowfield, especially at points that approached the discretized vortex sheet.[1] Not only would this enhance the versatility of vortex lattice methods,[2-4] but it would extend the force-free wake calculations[5-15] toward close-approach situations involving multiple components and their wakes. Such a capability would particularly benefit the analysis of high-lift configurations and the calculation of other close interference effects between

3

wings and vortex sheets (or vortices) such as occur in configurations with leading edge or tip-edge vortices.

Although the present paper deals with the near-field problem in two-dimensional flow, the extension for three-dimensional methods (particularly for methods having a force-free wake) is a major consideration throughout. The development of the discrete singularity technique is described in Section 2, and a study of the effects of various parameters in the model is given in Section 3. The calculations are based on a cambered Joukowski airfoil, and are primarily concerned with the detailed pressure distribution, but, as a means of indicating overall accuracy, coefficients of drag — which should be zero here — lift and pitching moment also are evaluated by integrating surface pressure effects.

2.0 Development of the Method

2.1 Basic Considerations

Existing surface singularity methods,[15-18] which are based mainly on piecewise constant singularity distributions on plane panels, have proved very powerful tools for predicting the potential flow characteristics of many configurations. However, in common with vortex lattice methods, their surface velocity calculations are essentially restricted to the control points. The present objective of calculating velocities at arbitrary points requires the near-field characteristics of a higher-order representation for both the singularity distribution and the airfoil geometry. Several higher-order surface singularity methods have been developed recently,[19-22] but they do not necessarily have the capability for calculating velocities at *arbitrary* surface points. Furthermore, high-order representation can be cumbersome to

4

apply to three-dimensional high-lift configurations with multiple force-free wakes. Also, it can be wasteful in computing effort when calculating velocities at even a small distance from the singularity sheet unless carefully controlled far-field models are included.

High-order representation adds little refinement to calculations in the far-field, yet many essentially far-field velocity calculations are performed when relaxing the trailing vortices in force-free wake applications.[6,7] On the other hand, the simplest model for far-field calculations is based on vortex-lattice theory; indeed, some very versatile methods have been developed,[2,12] but velocity calculations close to the discretized vortex sheets are restricted to special lines of approach.[1]

2.2 Submerged Singularities

One solution is to keep the singularity model simple and to place it *inside* the airfoil surface.[†] The airfoil contour is then treated as a streamline of the flow. Several flow calculation methods include internal singularities, either on the chord line or on the camber line. In the present work, internal singularities were developed such that they were placed on a "submerged" sheet closely related to the airfoil contour shape (Fig. 1). Obviously, the upper and lower parts of the sheet had a crossover upstream of the trailing edge, and so the affected parts were replaced by a single sheet extending from the crossover to the trailing edge along the mean line.

The effort to calculate three-dimensional wake rollup makes it preferable to use discrete singularities, but thin airfoils might require many

---

[†]This idea was suggested by Dr. V. J. Rossow in the Large-Scale Aerodynamics Branch at the NASA Ames Research Center.

singularities to maintain an accurate contour. For example, Fig. 2 shows pressure values calculated directly at *arbitrary* points on a cambered Joukowski airfoil which was represented by 41 submerged discrete vortices on a cosine spacing (described in Subsection 2.4). The vortex strengths were solved after specifying tangential flow at a set of control points on the airfoil surface.[7] The control points and vortices are indicated in the lower part of Fig. 2. The C_L based on circulation was 1.4% in error. The 120 pressure calculation points are not related to the vortex positions, and so the calculated pressure distribution shows large oscillations about the exact line (but it is much better than the distribution with the vortices on the surface). The submerged depth was 0.4Δ, whereas a depth of at least 1Δ would be required to reduce the errors to an acceptable level.[1] But the required number of vortices might then be unacceptably large (bearing in mind the three-dimensional case) especially if the close relationship between the submerged sheet and the airfoil contour is to be maintained. The calculated results downstream of the crossover indicate that such a relationship, i.e., separate sheets as opposed to a single mean-line sheet, might be important for this model. (The submerged depth is examined in Subsection 3.2.)

2.3 The Subvortex Technique

The subvortex technique[1] offers an attractive solution to this problem because it increases the number of vortices, but only where and when needed. Also, it is a logical model to use with the submerged singularity idea; for practical reasons, the subvortex technique gives a small region close to the singularity sheet where velocity errors are still appreciable.[1] This region is now enclosed in the airfoil contour. Thus, calculation points approaching

6

the airfoil surface never "see" the holes in the discretization because, locally, the number of subvortices increases to keep the point just outside the error region. As the calculation point moves from the surface, however, the vortex model quickly reverts to the basic discretization. The expression in Ref. 1 that controls the number of subvortices has been modified to improve the variation in NSV as the calculation point moves *along* the surface. The new expression is

$$NSV = FNS \left\{ \text{integer-part-of} \left[1 + \frac{0.5}{[(H/\Delta + (a/NRF\Delta)^2]} \right] \right\} \qquad (1)$$

where FNS, an (even) input parameter in the computer program, allows the density of the subvortex system to be varied. The number of subvortices is kept even to ensure that the control points, as well as the basic vortex locations, are midpoints in the subvortex system.[1] An upper limit is placed on the number of subvortices, based on a submerged depth factor (SDF), i.e.,

$$NSV_{max} = FNS \left(\text{integer-part-of } \frac{0.5}{SDF} \right) .$$

This prevents a runaway condition for the number of subvortices used near the trailing edge.

The same induced velocity expression is used throughout, i.e.,

$$\underline{V} = \Gamma \left(\frac{U\underline{i} + W\underline{k}}{2\pi} \right) \qquad (2)$$

where $U = a_z/a^2$, and $W = -a_x/a^2$. The vector $\underline{a} = (a_x\underline{i} + a_z\underline{k})$ is the position vector of the calculation point relative to the vortex being considered (basic vortex or subvortex) and $a^2 = \underline{a} \cdot \underline{a}$. The near-field treatment, therefore, is complicated only by the interpolation for the subvortex positions

7

and strengths; in the present work, linear interpolation was tried initially for both quantities to keep the model simple.

2.4 Vortex Positions

In the earlier work,[1] the vortices were positioned with equal spacing, but in the present study, the initial vortices (before submerging) were positioned on the airfoil surface using equal angle increments in a cosine equation applied to distance along the contour, i.e., the distance along the contour to the kth vortex point is

$$s_{v_k} = \frac{S(1 - \cos \theta_k)}{2} \tag{3}$$

where S is the length of contour associated with the interval $0 \leq \theta \leq \pi$. In this spacing system, half-angles separate the initial vortex positions from the control points where the boundary condition of tangential flow is specified. This is an adaptation of Lan's work;[23] it keeps the singularity strength distribution more uniform when passing through "difficult" regions such as leading and trailing edges and flap hinge lines. With this point distribution, the first control point is located at the trailing edge, and so the Kutta condition is applied by specifying the flow direction there, e.g., the direction along the mean line.

From their initial surface positions, the vortices are submerged along the local normal to the surface by a fraction of Δ, i.e., SDFΔ. The submerged depth factor, SDF, is constant over the whole contour except near the trailing edge, where it automatically decreases along the single sheet (Fig. 1). The control points remain on the airfoil contour except in the region very close to the trailing edge; here, corresponding upper and lower

8

control points are combined and moved to the mean line. Hence, the model adjacent to the trailing edge resembles a camber-line model, and alleviates the sensitivity of a surface vorticity method to trailing edge shape. Because of this modeling, there are more control points than unknown singularities, and so the equations are solved in a least-squares sense, using a NASA-Ames routine[24] based on the Householder method.[25]

For the initial model, the subvortices are placed on straight segments joining the basic vortices (Fig. 3). They are positioned with equal increments in θ; for example, between the kth and $(k + 1)$th basic vortices, the subvortex position vectors are:

$$\underline{r}_i = \underline{R}_{k+1}(n_i - 1) + \underline{R}_k n_i; \quad i = 1, 2, \ldots, NSV \qquad (4)$$

where: $n_i = (\cos \theta_k - \cos \theta s_i)/(\cos \theta_k - \cos \theta_{k+1})$; $s_i = \theta_k + (i - 0.5)\delta\theta$, and $\delta\theta = \Delta\theta/NSV$. The subvortex strength factor (i.e., subvortex strength/basic vortex strength) is

$$SSF_i = \frac{\sin \theta_i (1 - n_i)S \sin(\delta\theta/2)}{\Delta_k}$$

This distribution of subvortices approximates to a linear vorticity variation on the straight segments joining the basic vortices.

2.5 Equivalent Piecewise Constant Doublet Distribution

In three-dimensions, quadrilateral vortices are convenient for modeling arbitrary geometry configurations.[6,7,9] The present study, therefore, is based on the two-dimensional form of that model, viz., opposing vortex pairs (Fig. 3) which are equivalent to a piecewise uniform normal-doublet distribution. Such a model, forming a closed surface, requires one doublet panel

strength to be specified, otherwise the system is indeterminate. Accordingly, the upper panel adjacent to the crossover (Fig. 3) is specified to have zero strength. The boundary condition equation associated with the control point above the specified panel is still included in the system of equations, which is solved in the least-squares sense (Subsection 2.4). The resultant vortex strengths are

$$\Gamma_k = D_k - D_{k+1}; \quad k = 1, 2, \ldots, N$$

where D_k are the doublet panel strengths, i.e., the strengths of the opposing vortex pairs. (Note that D_{N+1} has been assumed zero.)

2.6 Initial Results

The singularity model was used to calculate surface pressures on the cambered Joukowski airfoil considered in Subsection 2.2. Incidence was $10°$, and the total number of basic vortices was 46 after submerging to a depth of 0.1Δ. The initial vortex positions (before submerging) were identical to those in Subsection 2.2. The near-field radius factor (NRF) was 5.0, following the work of Maskew,[1] and the subvortex parameter FNS in Eq. (1) was 2. The pressure distribution calculated at the same points as in Fig. 1 is quite good (see Fig. 4) except at the leading edge and near the crossover between the upper and lower submerged sheets. Just upstream of the crossover, the corresponding upper and lower vortices have almost identical sets of influence coefficients, and this produces ill-conditioning of the equations. In the solution, therefore, corresponding upper and lower vortices form increasingly strong opposing pairs as the junction is approached, and so a strong local flow is induced approximately in the direction of the mean line.

10

Although this increases the upper and lower surface calculated pressures (Fig. 4), the resultant strength between the corresponding vortices gives a smooth chordwise load distribution and an accurate lift and pitching moment, e.g., the calculated results from pressure integration using the trapezoidal rule are $C_L = 1.7064$ and $C_M = -0.5369$, compared with the exact values 1.6973 and -0.5391, respectively. The integrated drag coefficient (which should be zero) is -0.0098, i.e., an error of -0.57% of C_L.

The computing time for this calculation is four times that for the basic case with no subvortex technique. A small part of this increase (16%) is attributable to the larger number of vortices in the present case, viz., 46 cf. 41. The smaller submerged depth here results in fewer vortices being removed in the crossover region. The computing time could be reduced by storing the subvortex position vectors and strength factors; these quantities were recomputed each time in the present program.

2.7 Addition of Source Singularities

One way of explaining the pressure deviations near the subsurface crossover is that corresponding upper and lower vortices are trying to provide a thickness effect at the surface (as well as the lifting effect) from a small base. Source singularities, which are more suitable for providing thickness effects, were therefore combined with the vortices to remove the problem by providing a more suitable basic onset flow for the vortices. The source strengths are evaluated from a local linearized solution based on the relative slope between the airfoil surface and camber line:

$$\sigma_k = \frac{\Delta_k \underline{Vs}_k \cdot \underline{n}_k}{2\pi} \tag{5}$$

11

The source onset flow $\underline{V}s$ is a unit flow along the direction of the local camber line to facilitate the treatment of cambered airfoils. (A uniform onset flow was found unsuitable in such cases.) The model increases the computation time by 8%, yet the sources receive the same "subvortex" treatment as the basic vortices, i.e., Eq. (2) becomes:

$$\underline{V} = \left[\frac{\Gamma(U\underline{i} + W\underline{k}) + \sigma(W\underline{i} - U\underline{k})}{2\pi} \right]$$

"$\underline{\ }$" being the velocity contribution from a combined vortex/source. (In three dimensions the source treatment would be a more involved extension of the vortex equation.)

The sources, then, provide the vortices with a basic onset flow in which the thickness effects are approximately represented and this is particularly beneficial near the leading and trailing edge (Fig. 5). The pressure distribution from this model shows marked improvement (compare Figs. 4 and 5), but there is still a tendency for the pressure distribution to oscillate, particularly near the leading edge. Integrating the pressure distribution yields the following force and moment coefficients: $C_L = 1.7040$ (0.4% error), $C_D = -0.0069$ (0.4% of C_L), and $C_M = -0.5377$ (0.26% error).

2.8 Increase in the Density of the Subvortex System

To reduce the pressure oscillation near the leading edge, the number of subvortices was doubled (FNS = 4 in Eq. (1)). Figure 6 shows the resulting pressure distribution. Examination of the values shows the whole distribution is improved to the point that even the minor undulations, which can just be detected in the upper surface distribution in Fig. 5, are removed; but, though improved, the leading-edge overshoot in pressure is still there. Doubling

12

the factor FNS increases computation time by 53%, while the integrated force and moment coefficients show only minor improvements in accuracy. Increasing the number of subvortices to FNS = 8 did not significantly improve the distribution in Fig. 6.

2.9 Curved Subvortex "Sheet"

In a further attempt to remove the small leading-edge problem, a higher-order interpolation scheme (i.e., biquadratic) was applied for positioning the subvortices. Equation (4) was therefore replaced with

$$\underline{r}_i = g_1(n_i, n_1)\underline{R}_{k-1} + g_2(n_i, n_1, n_2)\underline{R}_k$$
$$+ g_2(1 - n_i, 1 - n_2, 1 - n_1)\underline{R}_{k+1} + g_1(1 - n_i, 1 - n_2)\underline{R}_{k+2} \quad (6)$$

where

$$g_1(n_i, n_1) = \frac{n_i(1 - n_i)^2}{[n_1(1 - n_1)]} \quad ;$$

$$g_2(n_i, n_1, n_2) = \frac{(1 - n_i)^2(n_1 - n_i)}{n_1} + \frac{n_i(1 - n_i)(n_2 - n_i)}{n_2} \quad ;$$

$$n_1 = \frac{-\Delta S_{k-1}}{\Delta S_k} \quad ; \quad n_2 = \frac{\Delta S_k + \Delta S_{k+1}}{\Delta S_k} \quad ; \quad n_i \text{ as in Eq. (4).}$$

(This is a cubic curve formed by a linear combination of two overlapping quadratic curves.)

The modified technique was applied to the same Joukowski airfoil as before, with FNS = 2. The resulting pressure distribution, shown in Fig. 7, indicates a small improvement in the leading-edge region (compare with Fig. 5 and examine the distances between pressure values near the leading edge). The computation time increased by 17% over the linear-interpolation case. This increase is larger than needed in practice because the biquadratic

13

interpolation was applied *throughout* the airfoil, whereas it is clearly not required over a substantial part of the contour (compare Figs. 5 and 7). In a practical method, the higher-order interpolation would be applied only in regions of high curvature and *only* when the maximum number of subvortices is being used in the segment.

The higher-order geometry routine slightly improved the accuracy for the integrated lift and pitching moment (the new errors being 0.34% and 0.24%, respectively), but the drag error was more than halved from -0.0069 to -0.0028 (i.e., 0.4% of C_L to 0.17% of C_L) as a result of the improved pressure distribution near the leading edge. Further improvement at the leading edge might be achieved using a higher-order strength distribution for the subvortices in the high curvature region. This would allow a closer representation of the extreme variation in vorticity that occurs at the leading edge in the present case (see also Subsection 3.1). Significantly, the pressure does not oscillate when the large peak is removed from the pressure distribution, e.g., Fig. 8 shows the pressure distribution for the same airfoil at zero incidence (C_D error in this case was 0.04% of C_L, i.e., 0.0002).

2.10 Pressure Integration

So far, the integrated values for C_L, C_M and C_D have been based on the trapezoidal rule applied to 120 calculated pressure values. A number of cases were computed for the configuration in Subsection 2.9 ($\alpha = 10°$) varying the number of calculation points but keeping the basic vortex/source model the same. The resulting integrated C_L, C_M and C_D errors are shown in Fig. 9. Minor variations are indicated for numbers down to 50 and even 25 in the case of lift and pitching moment. With only 25 calculation points on the airfoil,

14

however, the integrated drag coefficient has started to diverge; apart from this, the drag error is held below 0.5% of C_L and the lift and moment coefficient errors are below 0.5%. Small undulations occur because of the changing relationship between the calculation points and the small pressure oscillations seen in Fig. 7. Pressure integration for forces and moments was originally chosen as an overall guide to accuracy of the pressure distribution (particularly in the case of drag). The alternative, based on vortex strengths, appears less sensitive to the present modifications; for the case in Fig. 7, the lift based on circulation is only 0.1% in error.

2.11 Constraint Function

The vortex pair/doublet strength distribution has a very smooth form (Fig. 10) because it represents *integrated* vorticity over the surface. The smoothness (when plotted against doublet subscript k) is helped by the use of the cosine spacing (Subsection 2.4), which concentrates the singularities in the region of large vorticity gradient. A further contribution to the smoothness of the distribution is provided by the source singularities (Fig. 10). The resulting distribution can be represented by fairly simple interpolation functions with a view to reducing the number of unknowns. This principle has been widely used in the past, particularly in linearized theories using global functions covering, for example, a full wing span or chord. In the present work, a biquadratic constraint function (similar to Eq. (6) but with n based on the doublet subscript k instead of surface length) was briefly investigated to reduce the number of unknowns when the present method is extended to the three-dimensional form. The function was applied piecewise in a way similar to that in the constraint function

15

technique being developed in the NASA Ames POTFAN program.[26] The piecewise application (as opposed to a global one) should be more flexible in treating complicated configurations in three-dimensional flow. The full matrix of influence coefficients is still formed, but elements of the matrix are combined at selected pivotal positions in accordance with the constraint functions. After the pivotal values are solved, the complete set of doublet strengths is generated again using the constraint functions.

Figure 11 shows the calculated pressure distribution for the Joukowski airfoil represented by 46 vortices with the number of unknowns halved. (The corresponding full solution is in Fig. 7.) The C_L value decreased to 1.6783 (-1% error), and the computation time increased 14%; this increase accounts for the matrix manipulation time since the saving in the solution time at the present low level of unknowns is insignificant in comparison with the overall run time.

Further reductions in the number of unknowns caused substantial losses in the overall circulation and hence large errors in the pressure levels. The problem appears to be that the piecewise application of the constraint function decouples a large part of the doublet distribution from the Kutta condition control point, and although the general shape of the distribution is maintained (as in Fig. 10) the starting level at the trailing edge (which determines the circulation) falls as the number of unknowns is decreased. Development of this technique is continuing, and promises to remove the initial problem. The technique should lead to significant benefits for the three-dimensional method.

3.0 Parametric Study

A parametric study was performed to examine the following factors in the method: (a) the number of basic singularities, NBS; (b) the submerged depth factor, SDF; and (c) the near-field radius factor, NRF. Throughout the parametric study, the status of the method was as follows: (a) sources were present and their strengths solved in accordance with Eq. (5); (b) the biquadratic interpolation scheme was used for positioning the subvortices (Eq. (6)); (c) the constraint function routine was *not* used, i.e., the full solution was obtained directly; and (d) the factor on the number of subvortices, FNS in Eq. (1), was 2. The calculations were performed for the same cambered Joukowski airfoil as in Section 2. Incidence was again 10° and the pressures were calculated at the same 120 points. The base parameters, when they were not being varied, had the following values: NBS = 46, SDF = 0.1 and NRF = 5.0. Exceptions occurred in two situations: first, when varying NBS, the submerged *depth* was held constant and so the factor SDF varied; second, when varying SDF, the number of basic singularities (NBS) varied slightly because of the changing length of the single sheet near the trailing edge.

3.1 Effect of Number of Basic Singularities

The number of basic singularities (i.e., combined vortex/sources), NBS, was varied from 19 to 92 using a constant submerged depth. This depth corresponded to an SDF value of 0.1 in the base case with NBS = 46. Figure 12 shows the pressure distribution for NBS = 19; using so few vortices would clearly be an advantage in three-dimensional applications. The calculated

17

pressure values are surprisingly good over most of the airfoil, but an oscillation is present near the leading edge. This pressure oscillation decreases as NBS increases, and virtually disappears when NBS = 92. This result indicates that a closer representation of the conditions near the leading edge might improve the solution when using a small value for NBS; since the model already represents geometric curvature, and since we have already tried increasing the effective number of singularities (Subsection 2.8), then an improvement might be obtained by using a higher-order distribution for the subvortex strengths near the leading edge (see also Subsection 2.9).

Figure 13 shows the errors in the calculated values for the lift, drag and pitching moment coefficients for different values of NBS. These quantities undulate slightly because of the numerical integration scheme, coupled with the changing relationships between the (fixed) calculation points and the (varying) vortex/source locations. Nevertheless, the error levels appear to be bounded: C_L and C_M are well within 1% error, and the C_D error is below 0.5% of C_L, even with only 19 basic singularities.

The computation time does not vary much for small values of NBS, e.g., the time with NBS = 19 is only 7% lower than the time with NBS = 46. The reason is that with a constant submerged depth, the required number of subvortices increases as the number of basic vortices decreases. The times for forming the matrix of influence coefficients and for solving the equations do vary with NBS, however, and although these form only a small part of the total time (i.e., less than 25%) for low NBS values, when NBS = 91 these contributions cause an increase of 64% in total time over that for the base case (NBS = 46).

3.2 Effect of Submerged Depth

The submerged depth factor, SDF, was varied from 0.025 to 0.4 on the basic case. Two of the resulting pressure distributions for SDF = 0.025 and 0.4 are shown in Figs. 14(a) and 14(b), respectively. Figure 7 shows the corresponding distribution for SDF = 0.1. With the small submerged depth (Fig. 14(a)), the leading-edge pressure oscillation is made worse — possibly because the "linear vorticity" distribution is closer to the surface — but the pressures in the trailing-edge region are even better than in the basic case with SDF = 0.1 (compare with Fig. 7).

The larger submerged depth (Fig. 14(b)) gives a smoother pressure distribution near the leading-edge — but with a too-high value; at the trailing edge, however, the pressure distribution has collapsed. A value for SDF between 0.05 and 0.1 (for NBS = 46) gives the best pressure distribution. Computing time should be taken into consideration, however. As the submerged depth decreases, the number of subvortices must increase, and so computing time increases rapidly, especially for SDF values below 0.1, e.g., the time for SDF = 0.05 is 35% higher than that for SDF = 0.1.

Figure 15 shows how the integrated force and moment coefficients vary with submerged depth. As SDF increases, C_D and C_M errors become rapidly worse — probably because of the deteriorating pressure distribution near the trailing edge. SDF does not appear to affect C_L appreciably.

3.3 Effect of Near-Field Radius

The near-field radius factor, NRF, when multiplied by the Δ value of a basic vortex, defines a circle centered on that vortex. Whenever a velocity calculation point comes inside the circle, then that basic vortex is modified

19

by the subvortex technique. The near-field radius was examined for a simple case,[1] and on the basis of that, an NRF value of 5 was used for initial work here. To examine its effect in the airfoil application, NRF was varied from 1 to 7. Figure 16 shows the pressure distribution with NRF = 1 — which is clearly too small. The calculated pressure distribution at the arbitrary points improves as NRF increases, but there is little visual change in the distributions for NRF values above about 3. Computing time decreases rapidly as NRF is reduced; a value of 3 instead of 5 for NRF gives a time saving of 30%.

Figure 17 shows the effect of NRF on the force and moment errors from the pressure integration. They show excellent convergence characteristics as NRF increases, although C_L appears to be converging towards an error of the order of 0.5%. The error in C_L based on circulation, however, converges towards zero.

4.0 Conclusions

The combination of a near-field subvortex technique with a concept that places the singularities inside the airfoil has resulted in a method by which accurate pressures (and velocities) can be calculated directly (i.e., without interpolation) at any arbitrary point on the airfoil surface. The method is essentially a numerical integration procedure, but, by approaching it via the vortex lattice model, a useful set of rules and automatic procedures has been developed which makes the method accurate as well as efficient when moving from near- to far-field regions. The calculations were enhanced by combining sources with the vortices.

The results obtained so far indicate that the number of b sic singularities used to represent a section should be of the order of 40 o. 50. However, the results also suggest that the use of a higher-order strength variation for the subvortices in regions of high pressure gradient might allow the number to be decreased — possibly as low as 20.

Bearing in mind accuracy and computing effort, the optimum values for the submerged depth and for the near-field radius would appear to be of the order of 0.1Δ and 3Δ, respectively. Computing time penalties quoted herein for the various parametric changes and developments are, in general, on the pessimistic side. There is considerable potential for improving the test method to reduce computation effort, particularly in connection with the subvortex system.

The method can be extended to three dimensions for application to vortex lattice based methods, and should then allow close-approach situations associated with multiple components and force-free wake calculations.

5.0 References

[1]Maskew, B., A Subvortex Technique for the Close Approach to a Discretized Vortex Sheet," NASA TM X-62,487, Sept. 1975.

[2]Ruppert, P. E., "Theoretical Characteristics of Arbitrary Wings by a Non-planar Vortex Lattice Method," D6-9244, The Boeing Co., 1964.

[3]Margason, R. J. and Lamar, J. E., "Vortex Lattice Fortran Program for Estimating Subsonic Aerodynamic Characteristics of Complex Planforms," NASA TN D-6142, Feb. 1971.

[4]Tulinius, J., Clever, N., Nieman, A., Dunn, K., and Gaither, B., "Theoretical Prediction of Airplane Stability Derivations at Subcritical Speeds," NASA CR-132681, 1975.

[5]Belotserkovskii, S. M., "Calculation of the Flow Around Wings of Arbitrary Planform over a Wide Range of Angles of Attack," NASA TTF-12,291, May 1967.

[6]Maskew, B., "On the Influence of Camber and Non-Planar Wake on the Airfoil Characteristics in Ground Effect," Loughborough University of Technology, Leics, England, TT7112, Oct. 1971. (See also ARC 33950, 1973, Aeronautical Research Council, London.)

[7]Maskew, B., "Numerical Lifting Surface Methods for Calculating the Potential Flow about Wings and Wing-Bodies of Arbitrary Geometry," Ph.D. thesis, Department of Transport Technology, Loughborough University of Technology, Leics, England, 1972.

[8]Lind, I. A., "A Non-Linear Vortex Lattice Method Applicable to Three-Dimensional Wing Systems with Rolled Up Vortex Wakes in Low Subsonic Flow," FI43, The Royal Institute of Tech., Stockholm, Sweden, 1973.

[9]Maskew, B., "The Calculation of Potential Flow Aerodynamic Characteristics of Combined Lifting Surfaces with Relaxed Wakes," YAD 3192, Hawker-Siddeley Aviation Ltd., Brough, North Humberside, England, Sept. 1973.

[10]Rehbach, C., "Calculation of Flows Around Zero Thickness Wings with Evolutive Vortex Sheets," NASA TTF-15,183, 1973.

[11]Mook, D. T. and Maddox, S. A., "Extension of a Vortex Lattice Method to Include the Effects of Leading-Edge Separation," *Journal of Aircraft*, Vol. 11, No. 2, Feb. 1974, pp. 127-128.

[12]Summa, J. M., "Potential Flow about Three-Dimensional Streamlined Lifting Configurations, with Application to Wings and Rotors," SUDAER Report No. 485, Stanford Univ., Calif., Sept. 1974.

[13]Hackett, J. E. and Evans, M. R., "Vortex Wakes Behind High-Lift Wings," *Journal of Aircraft*, Vol. 8, No. 5, May 1971, pp. 334-340.

[14]Butter, D. J. and Hancock, G. J., "A Numerical Method for Calculating the Trailing Vortex System Behind a Swept Wing at Low Speed," *The Aeronautical Journal*, Vol. 75, No. 728, Aug. 1971, pp. 564-568.

[15]Labrujere, Th. E., "A Numerical Method for the Determination of the Vortex Sheet Location Behind a Wing in Incompressible Flow," TR 72091 U, National Aerospace Laboratory (NLR), Amsterdam, The Netherlands, July 1972.

[16]Rubbert, P. E., Saaris, G. R., Scholey, M. B., and Standen, N. M., "A General Method for Determining the Aerodynamic Characteristics of Fan-Wing Configurations, Vol. I, Theory and Applications," USAAVLABS TR 67-61A, Dec. 1967.

. [17]Woodward, F. A., Dvorak, F. A., and Geller, E. W., "A Computer Program for Three-Dimensional Lifting Bodies in Subsonic Flow," Rep. USAAMRDL-TR-74-18, U.S. Army Air Mobility Research and Development Laboratory, Ft. Eustis, Virginia, April 1974.

[18]Hess, J. L., "Calculation of Potential Flow About Arbitrary Three-Dimensional Lifting Bodies," MDC J5679-01, McDonnell Douglas Corp., Long Beach, Calif., Oct. 1972.

[19]Argyris, J. H. and Scharpf, D. W., "Two and Three-Dimensional Potential Flow by the Method of Singularities," *The Aeronautical Journal*, Vol. 73, Nov. 1969, pp. 959-9 .

[20]Roberts, A. and Rundle, K., "The Computation of First-Order Compressible Flow About Wing-Body Configurations," AERO MA 20, British Aircraft Corp., Weybridge, England, Feb. 1973.

[21]Hess, J. L., "The Use of Higher Order Surface Singularity Distributions to Obtain Improved Potential Flow Solutions for Two-Dimensional Lifting Airfoils," *Computer Methods in Applied Mechanics and Engineering*, 5, 11-35, North Holland Publishing Co., Amsterdam, 1975.

[22]Mercer, J. E., Weber, J. A., and Lesford, E. P., "Aerodynamic Influence Coefficient Method Using Singularity Splines," NASA CR-2423, May 1974.

[23]Lan, C. E., "A Quasi-Vortex Lattice Method in Thin Wing Theory," *Journal of Aircraft*, Vol. 11, No. 9, Sept. 1974, pp. 518-527.

[24]Davis, J. E., Bannett, W. B., and Medan, R. T., "NASA Ames 3-D Potential Flow Analysis System (POTFAN) Equation Solver Code (SOLN)," NASA TM X-73,074, to be published.

[25]Franklin, J. N., *Matrix Theory*, Prentice-Hall, 1968.

[26]Medan, R. T. and Davis, J. E., private communication.

Fig. 1 Submerged singularity model with discrete vortices.
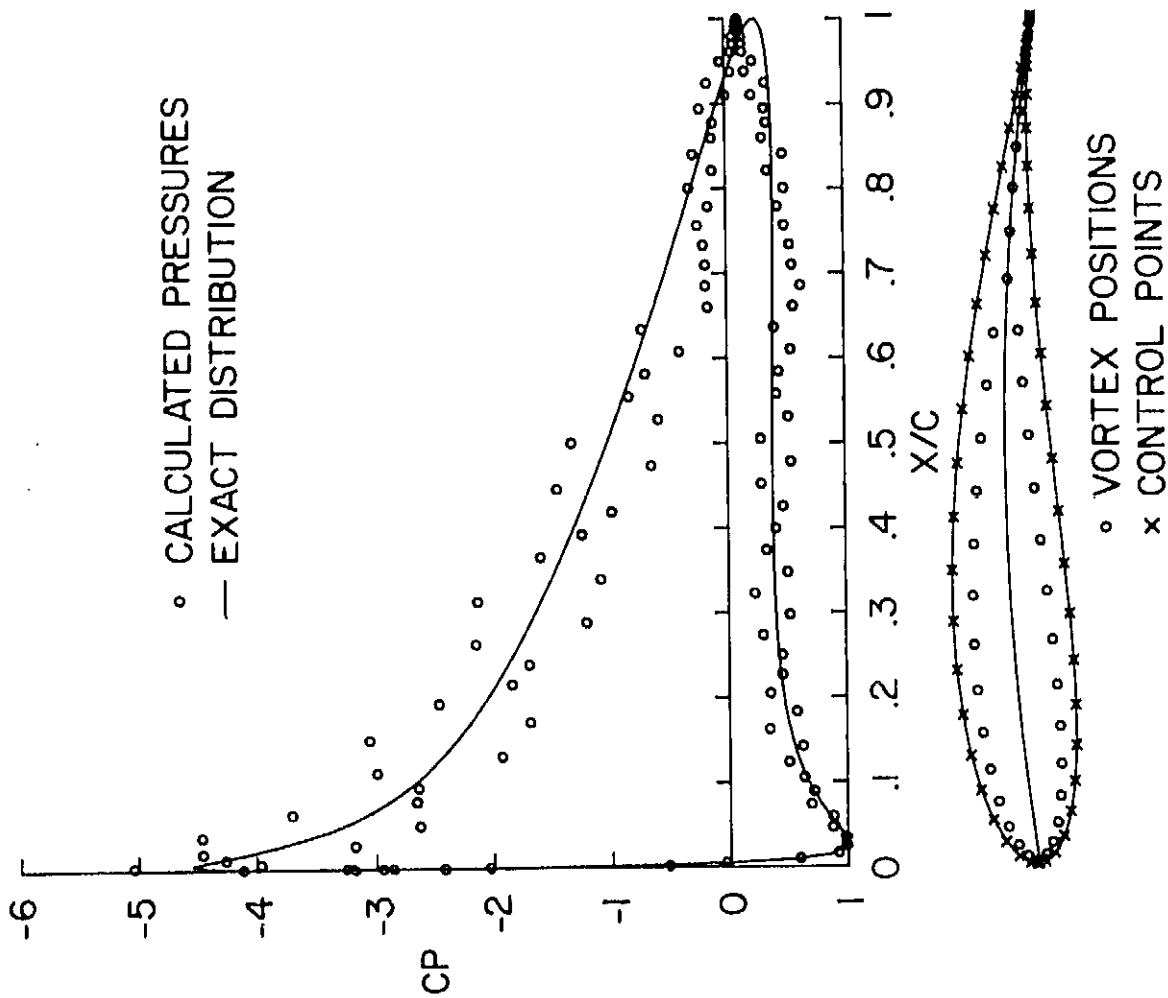
Fig. 2 Pressures calculated at arbitrary points on a Joukowski airfoil at 10° incidence. Model: submerged vortices only; NBS = 41; $SDF = 0.4$.

kth PANEL WITH PAIR OF EQUAL BUT OPPOSITE VORTICES
OR EQUIVALENT CONSTANT DOUBLET DISTRIBUTION (STRENGTH D_k)

BASIC VORTEX STRENGTH
$\Gamma_k = D_k - D_{k+1}$

ZERO STRENGTH DOUBLET
PANEL HERE

$-D_k$ $+D_k$ D_{k+1}

KUTTA CONDITION APPLIED
AT TRAILING-EDGE

SUBVORTICES ASSOCIATED WITH BASIC VORTICES
ARE PLACED ON THE "SUBMERGED SHEET"
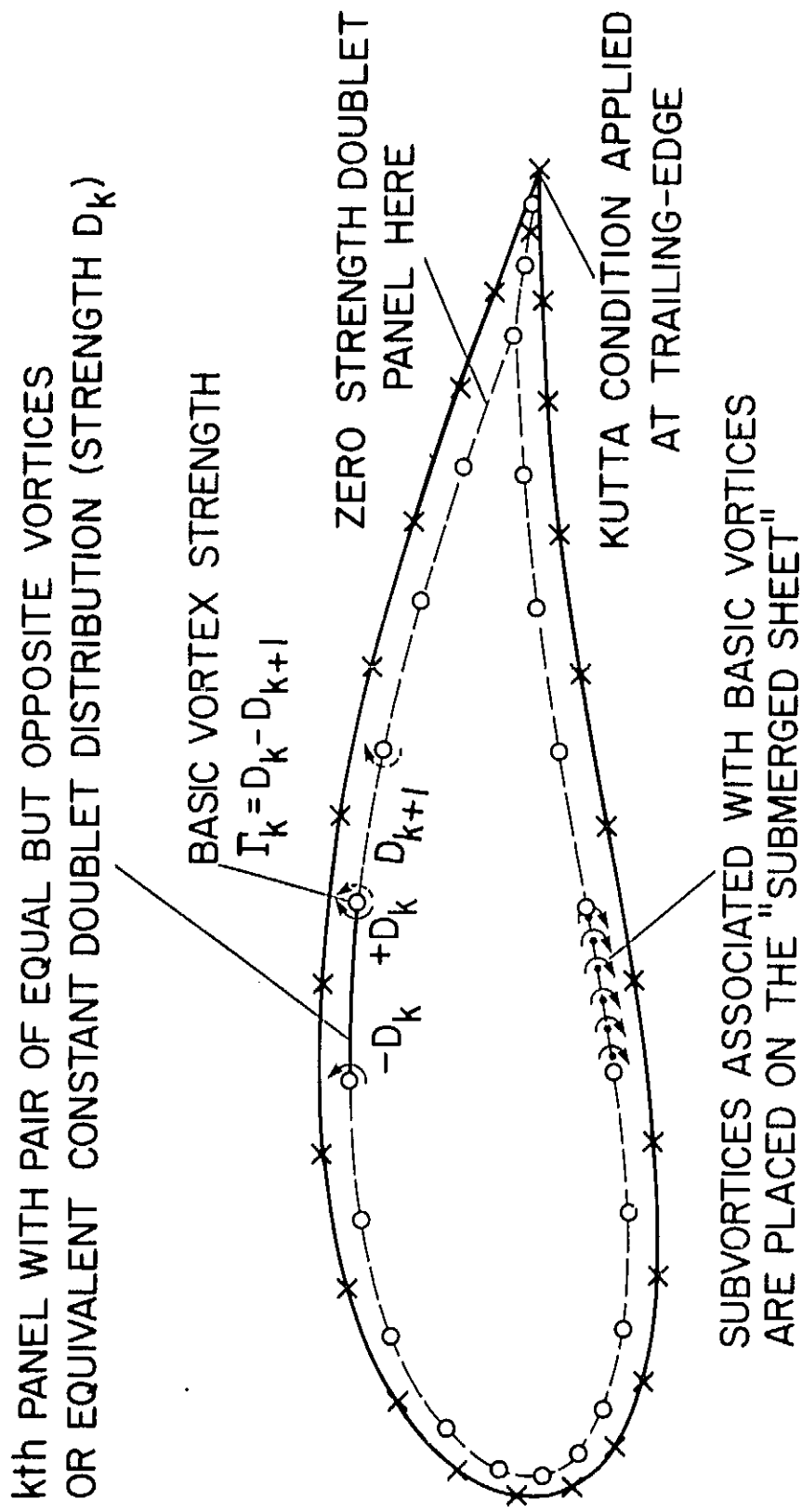
Fig. 3 Equivalent piecewise constant doublet model.
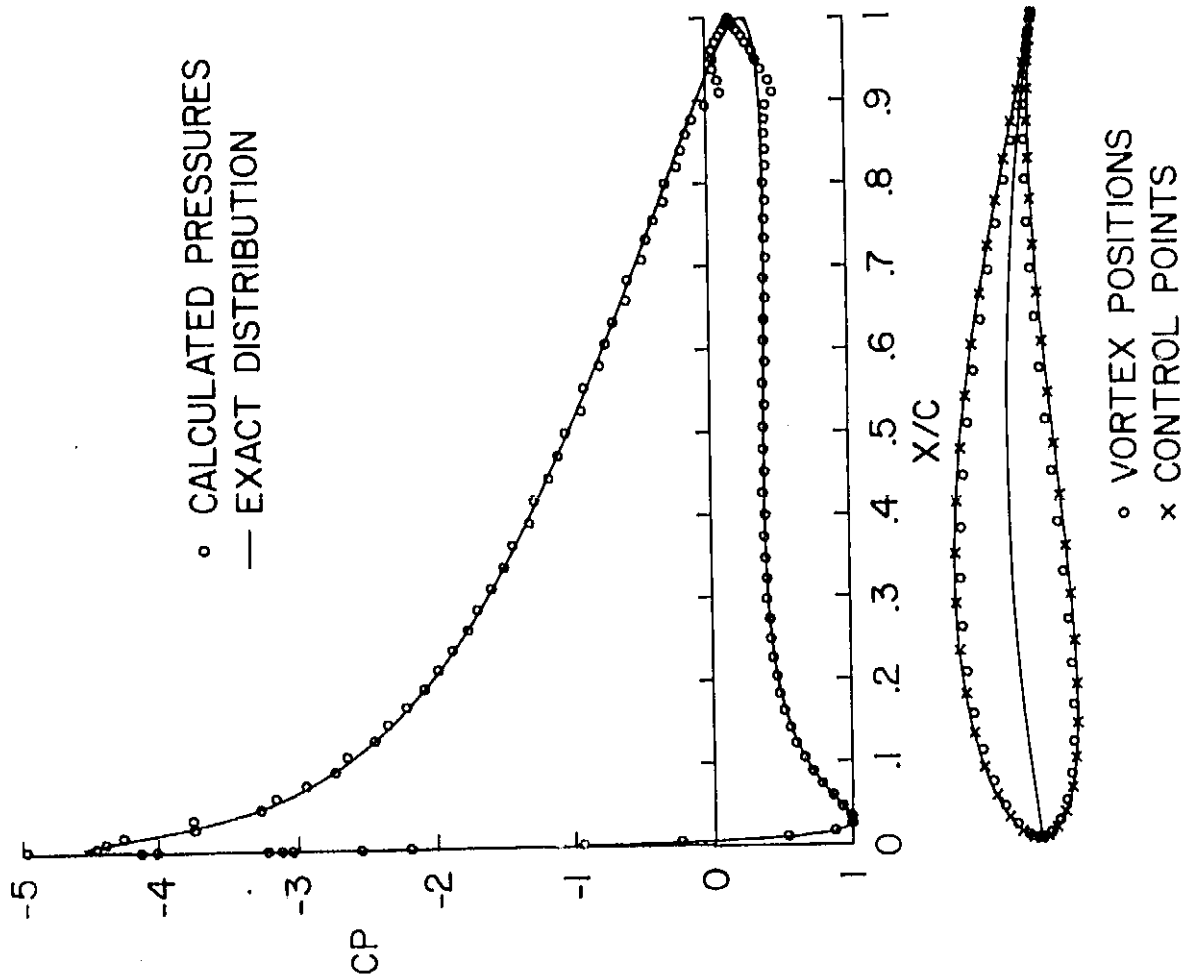
Fig. 4 Pressures calculated at arbitrary points on a Joukowski airfoil at 10°
incidence. Model: submerged vortices with subvortex technique applied
(linear interpolation for position); NBS = 46; SDF = 0.1; NRF = 5.0; FNS = 2.
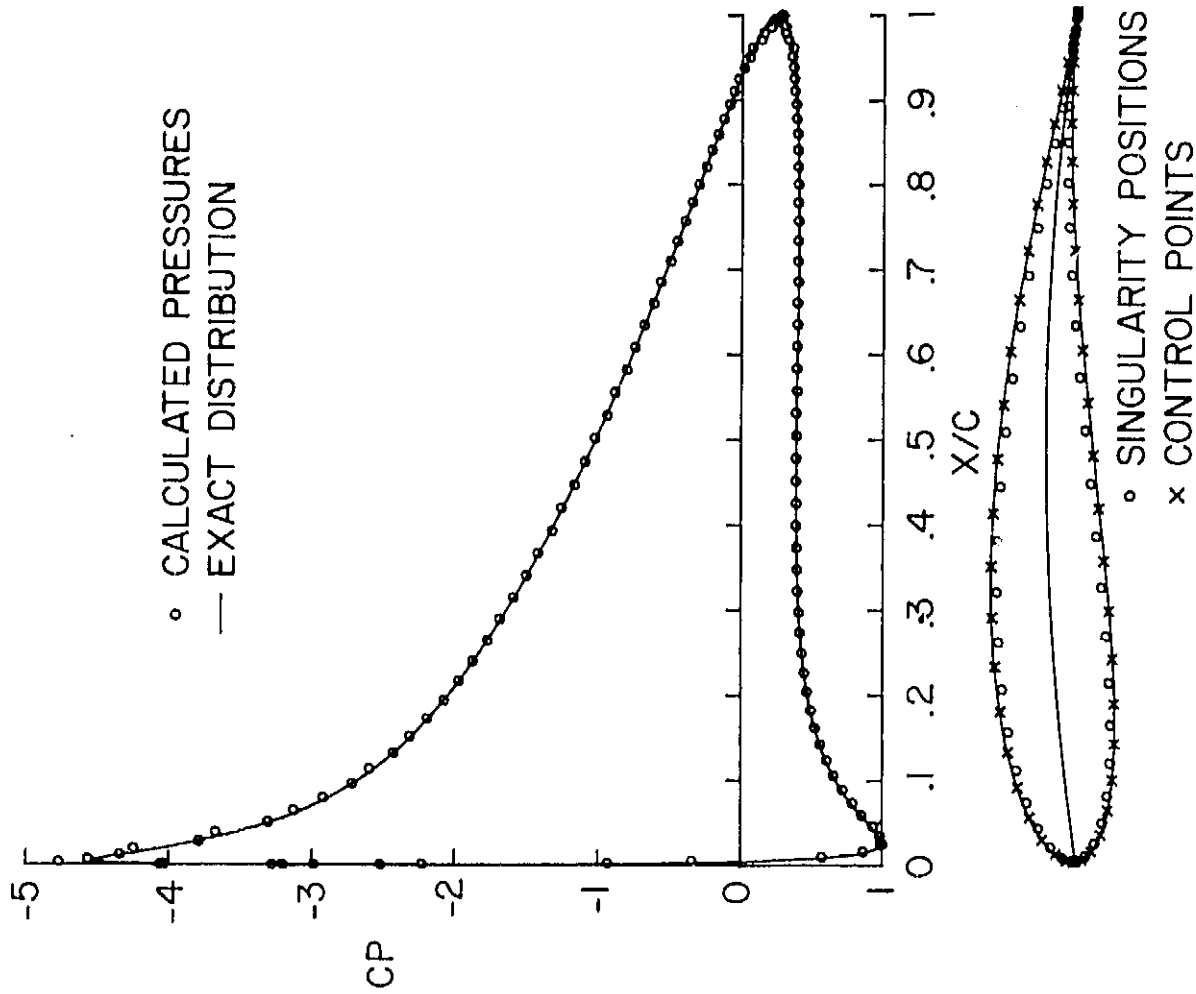
Fig. 5 Pressures calculated at arbitrary points on a Joukowski airfoil at 10° incidence. Model: submerged vortices and sources (coincident) with subvortex technique applied (linear interpolation for position); NBS = 46; SDF = 0.1; NRF = 5; FNS = 2.
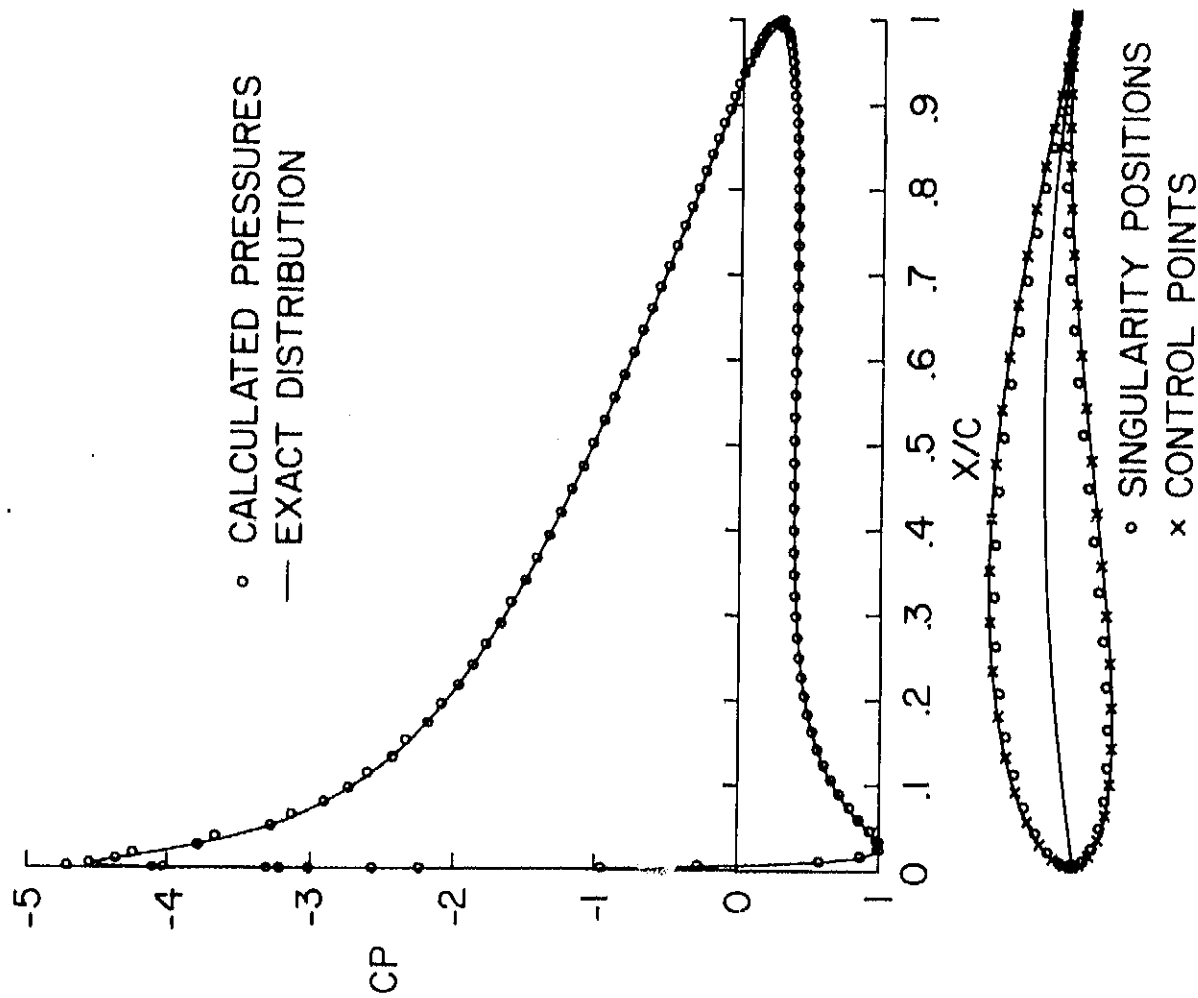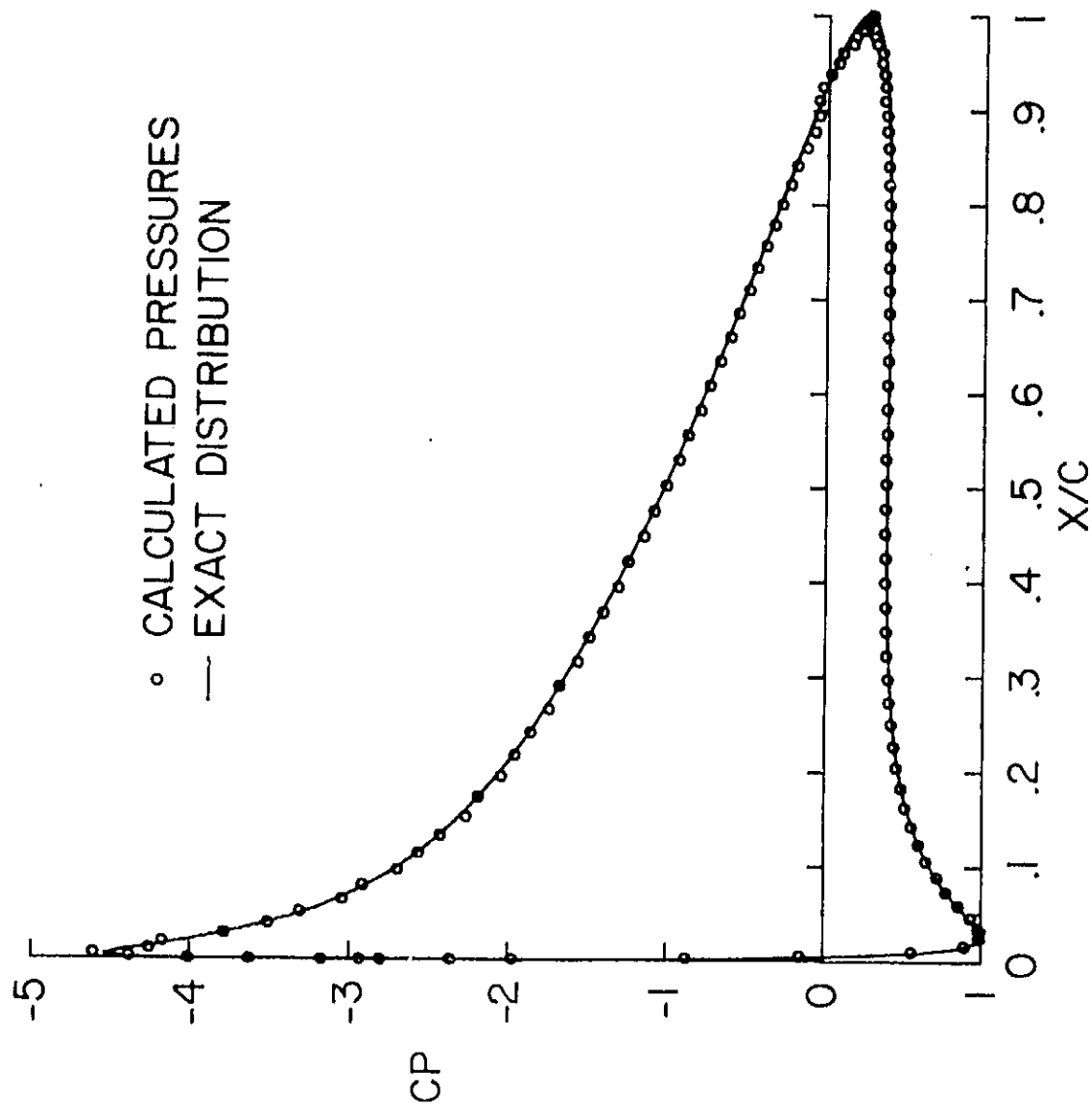
Fig. 6 Pressures calculated at arbitrary points on a Joukowski airfoil at 10° incidence. Model: as in Fig. 5, but with number of subvortices doubled (FNS = 4).
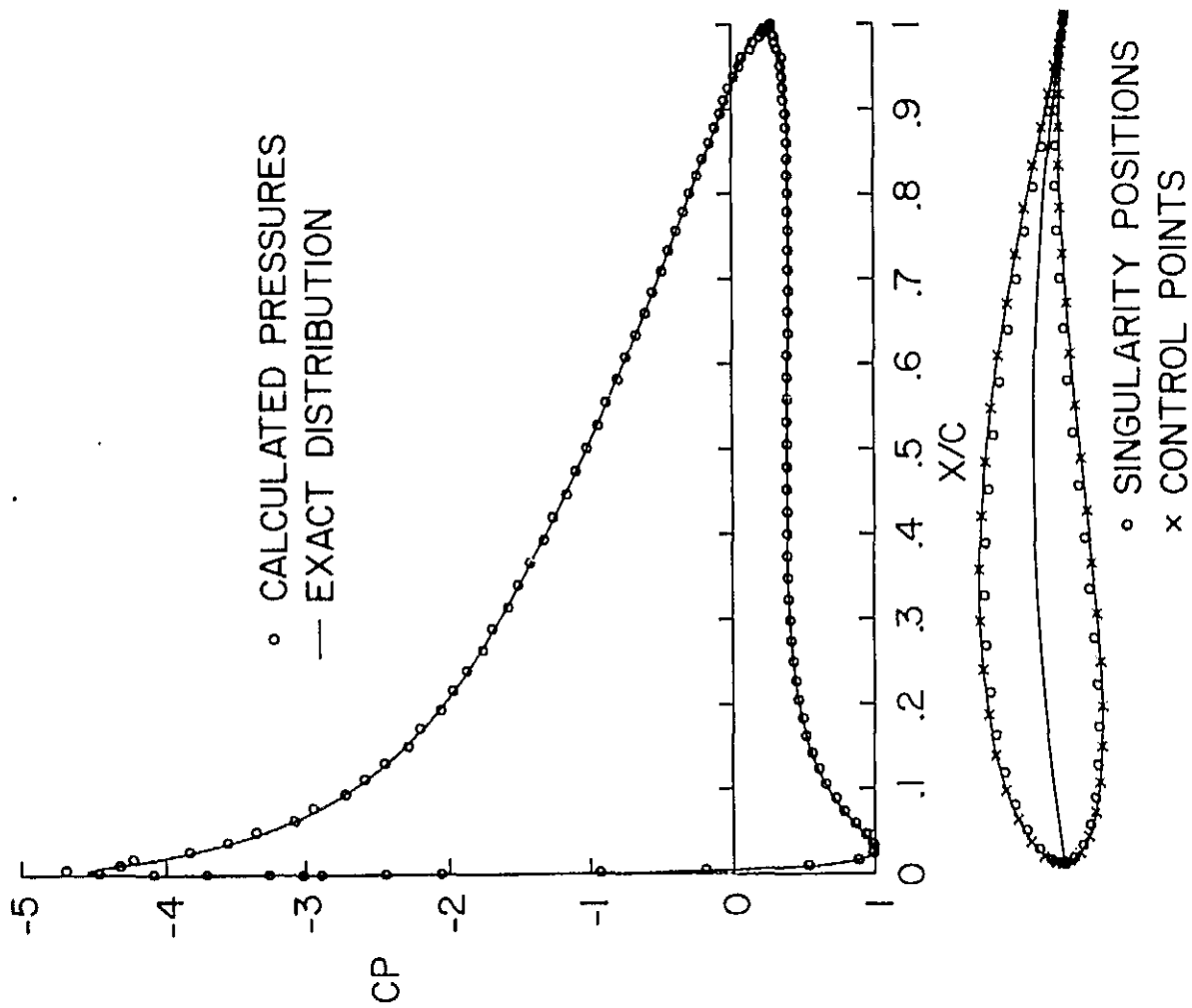
Fig. 7 Pressures calculated at arbitrary points on a Joukowski airfoil at 10° incidence. Model: as in Fig. 5, but with biquadratic interpolation for subvortex positions; NBS = 46; SDF = 0.1; NRF = 5; FNS = 2.
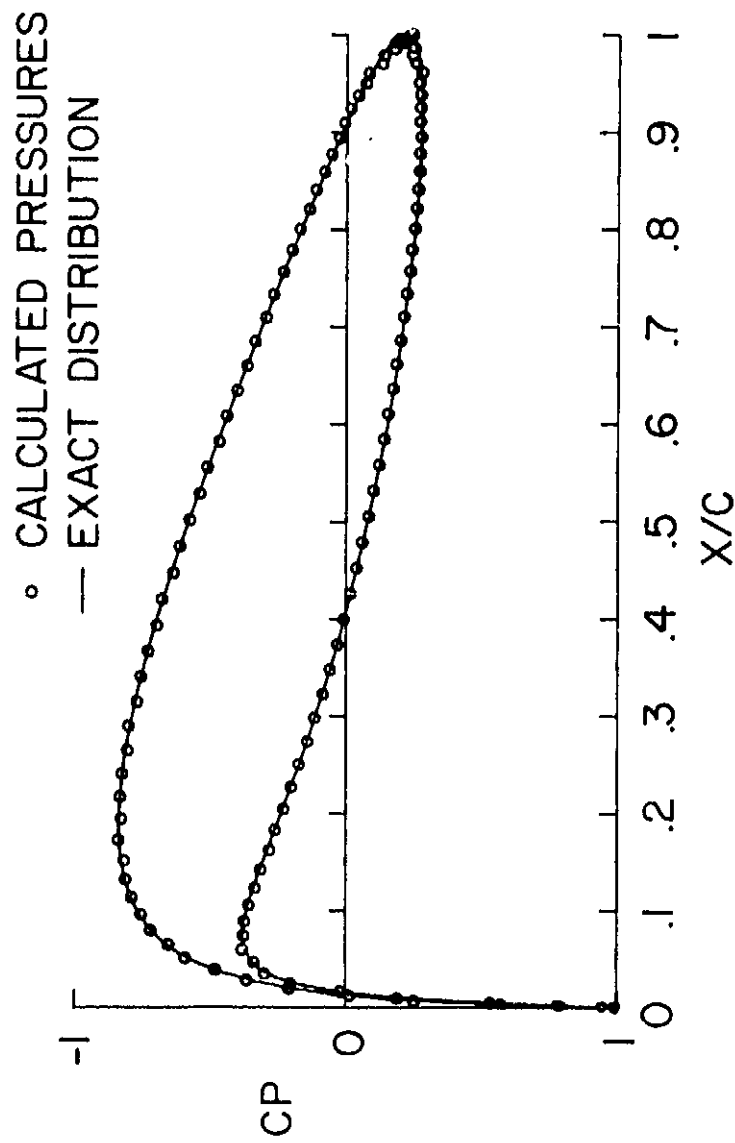
Fig. 8 Pressures calculated at arbitrary points on a Joukowski airfoil at
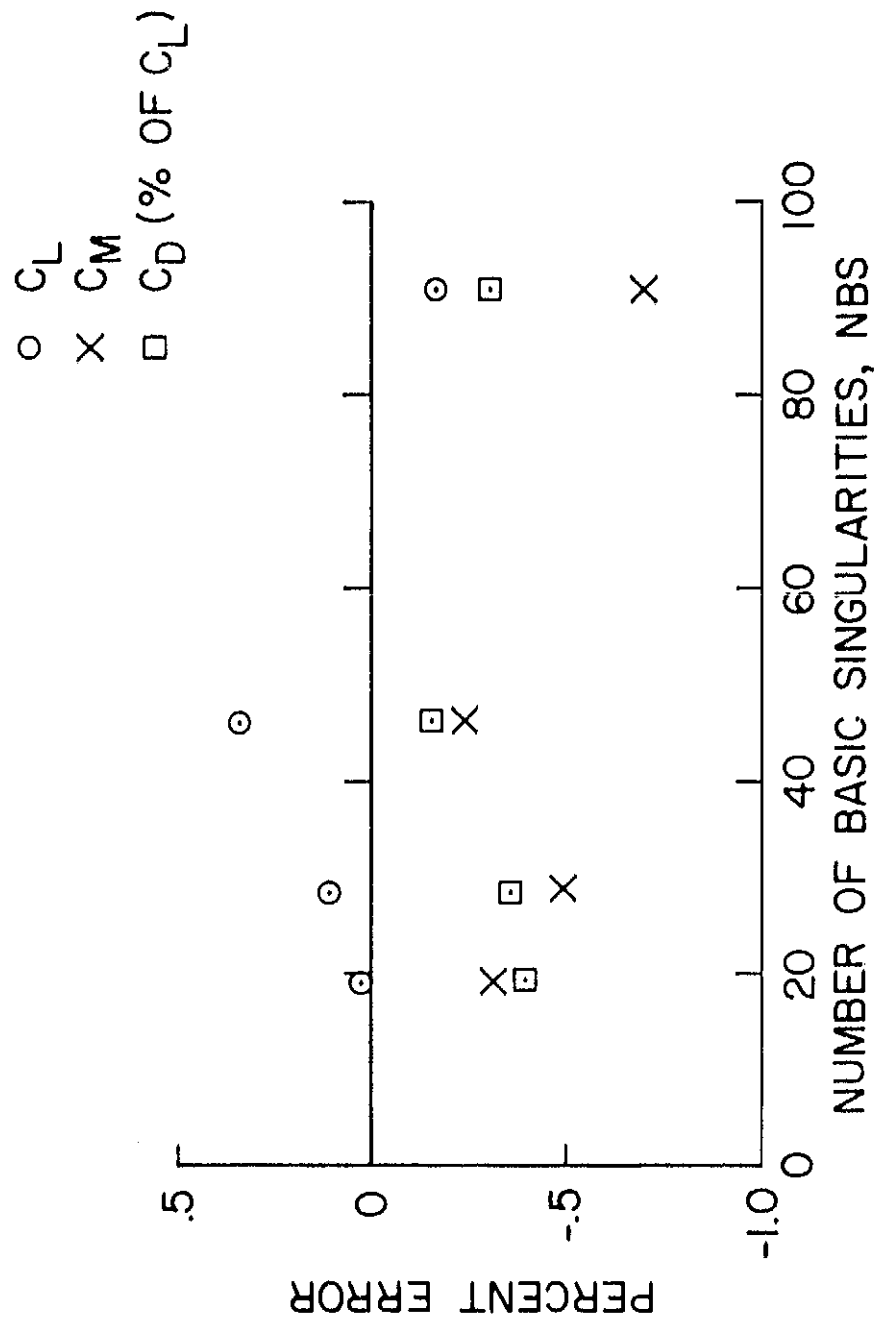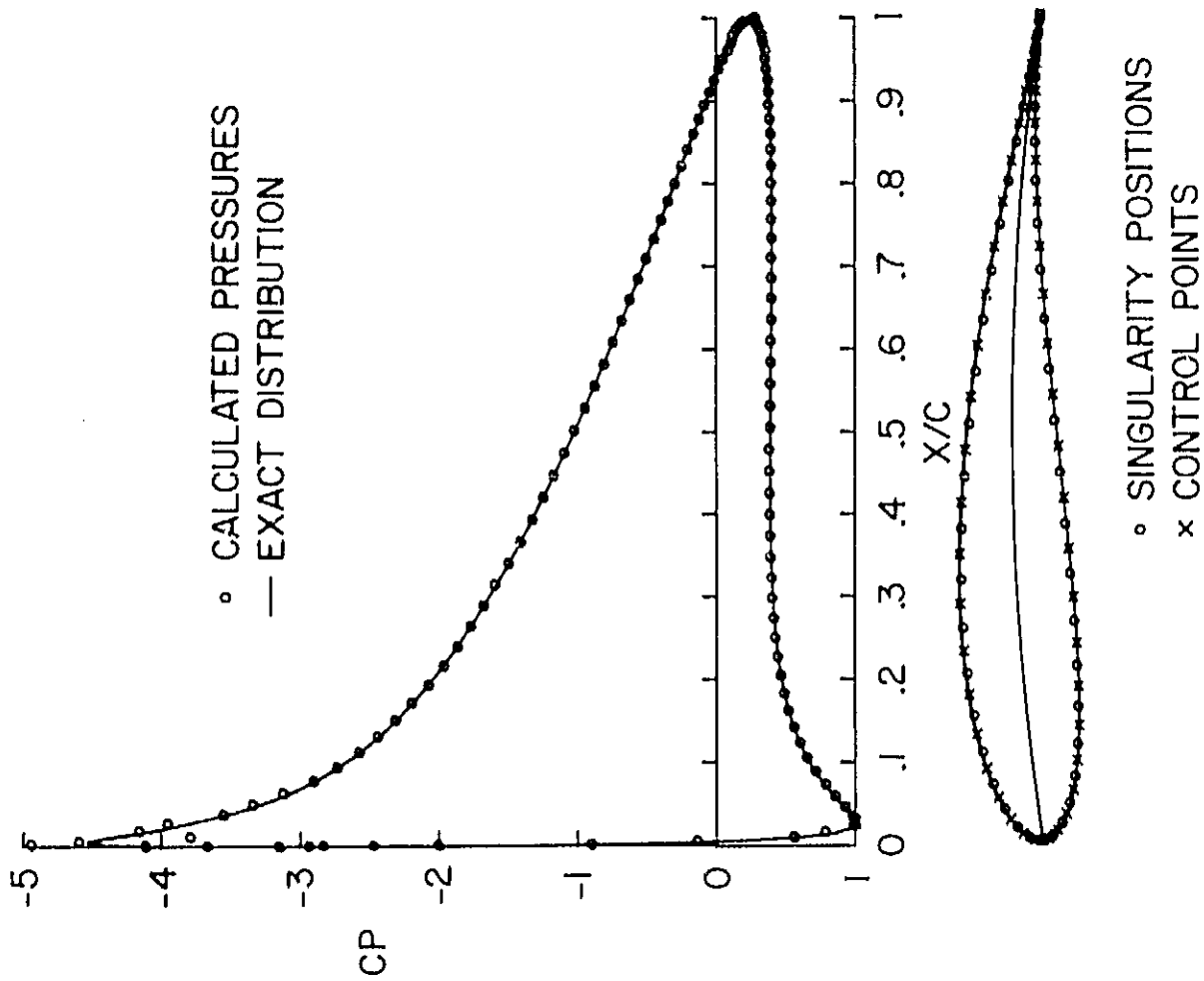zero incidence. Model: as in Fig. 7.
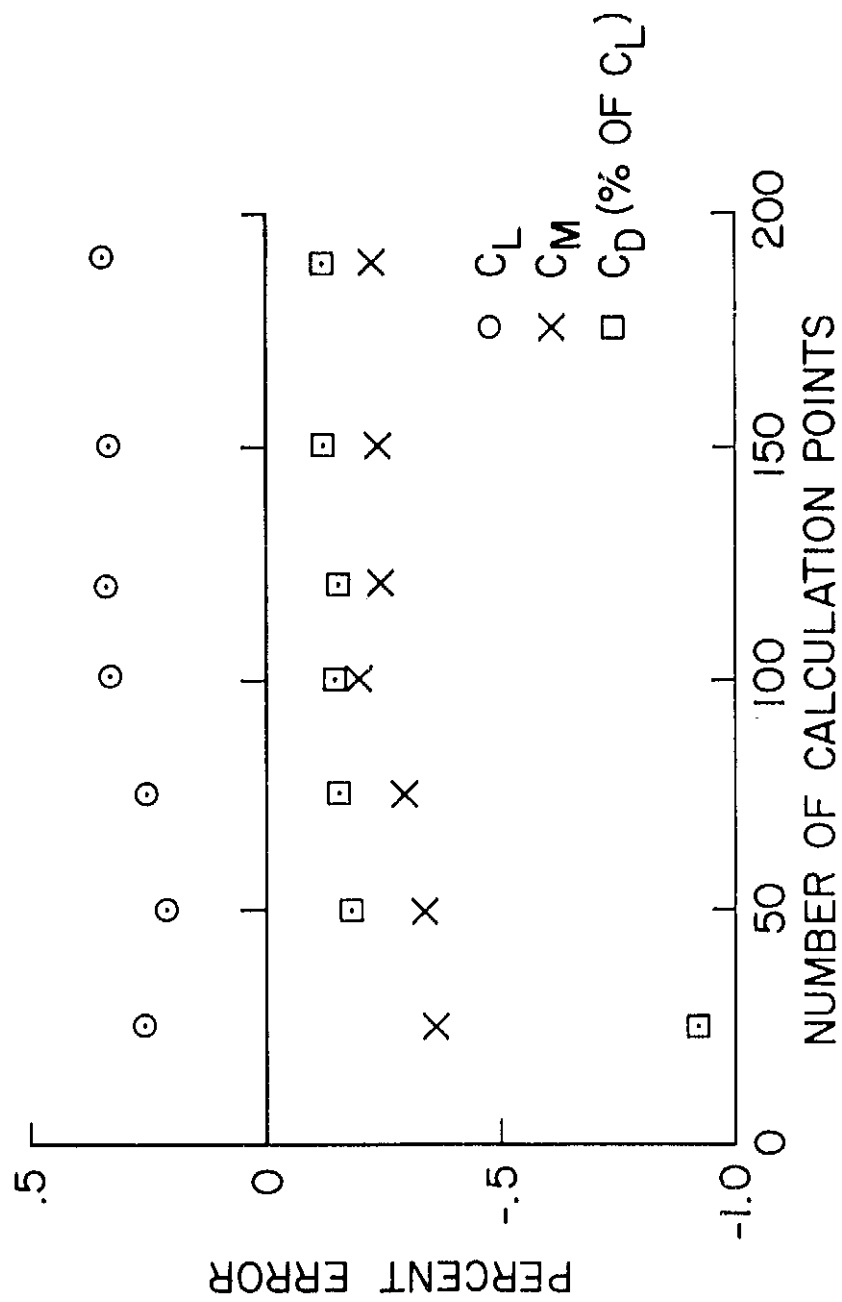
Fig. 9 Effect of the number of calculation points on the errors in the inte-
grated force and moment coefficients. Basic case as in Fig. 7.
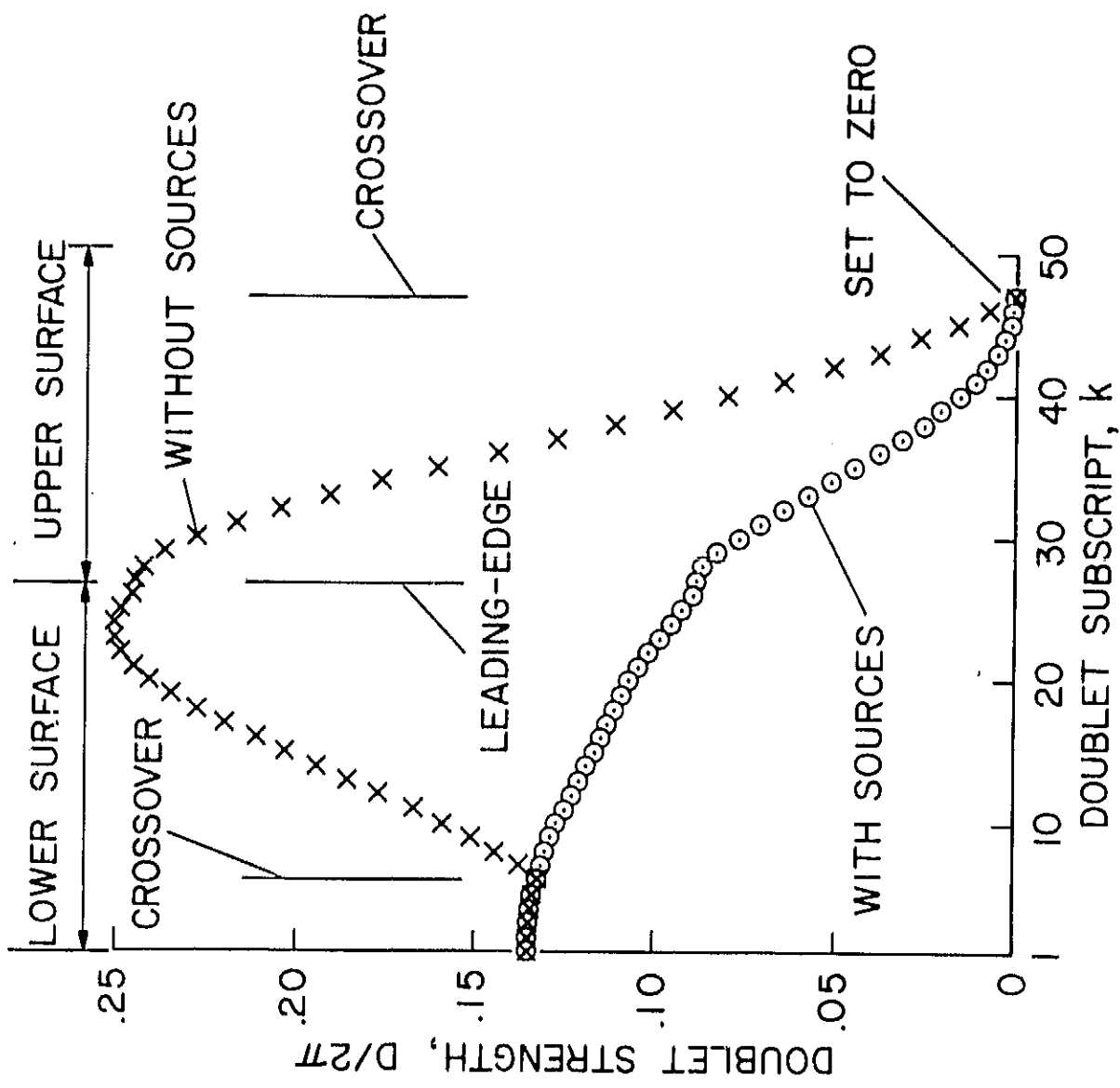
Fig. 10 Doublet strength distribution with and without sources present. (Cases in Figs. 4 and 5, respectively.)

Fig. 11 Pressures calculated at arbitrary points on a Joukowski airfoil at 10° incidence. Model: as for Fig. 7, but basic number of unknowns halved by using a constraint function.
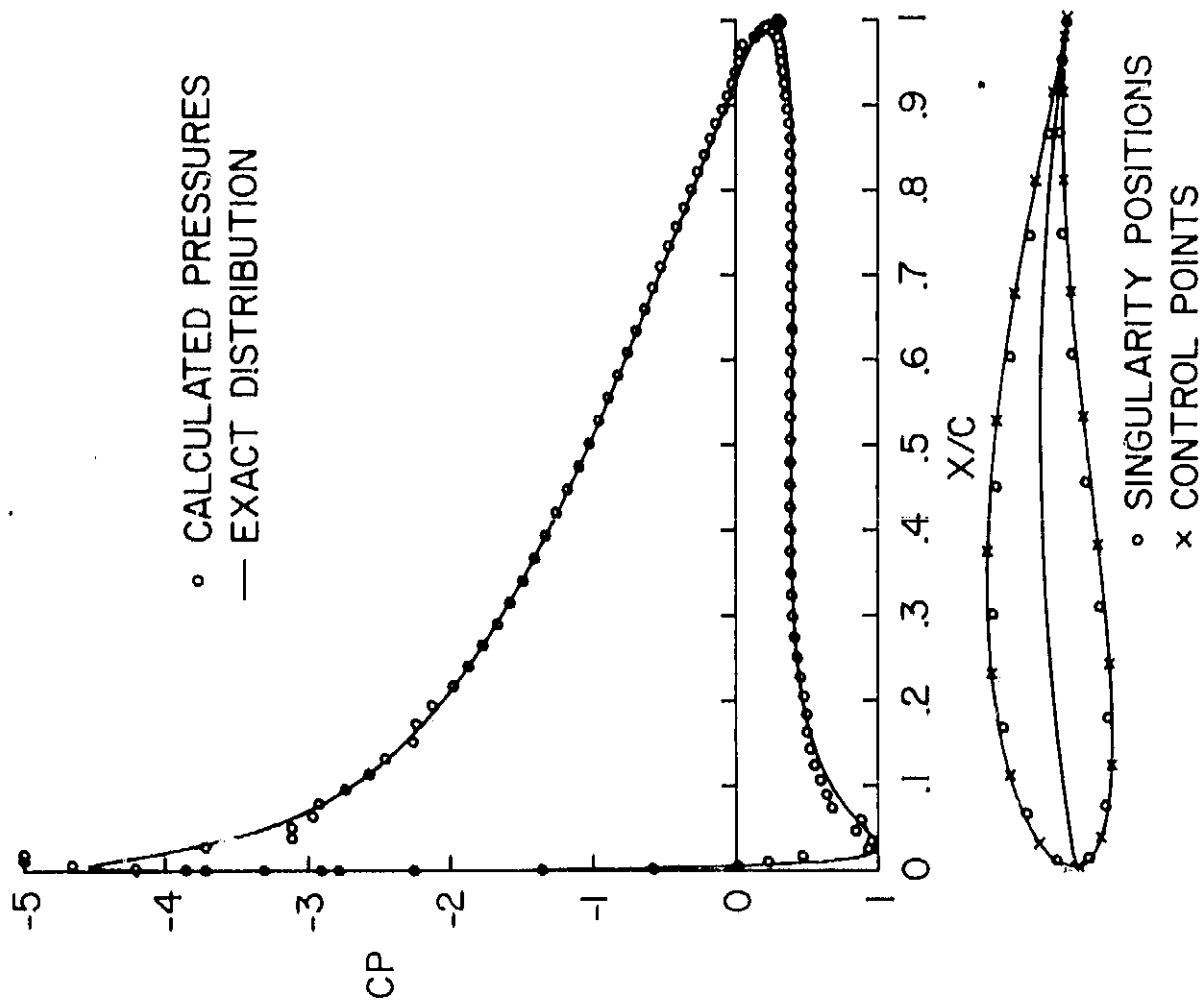
Fig. 12 Pressures calculated at arbitrary points on a Joukowski airfoil at 10°. Model: as in Fig. 7 but NBS = 19.

Fig. 13 Effect of number of basic singularities, NBS, on the errors in the integrated force and moment coefficients. Basic case as in Fig. 7.

Fig. 14 Pressures calculated at arbitrary points on a Joukowski airfoil at 10° incidence. Model: as in Fig. 7, but with different submerged depths.
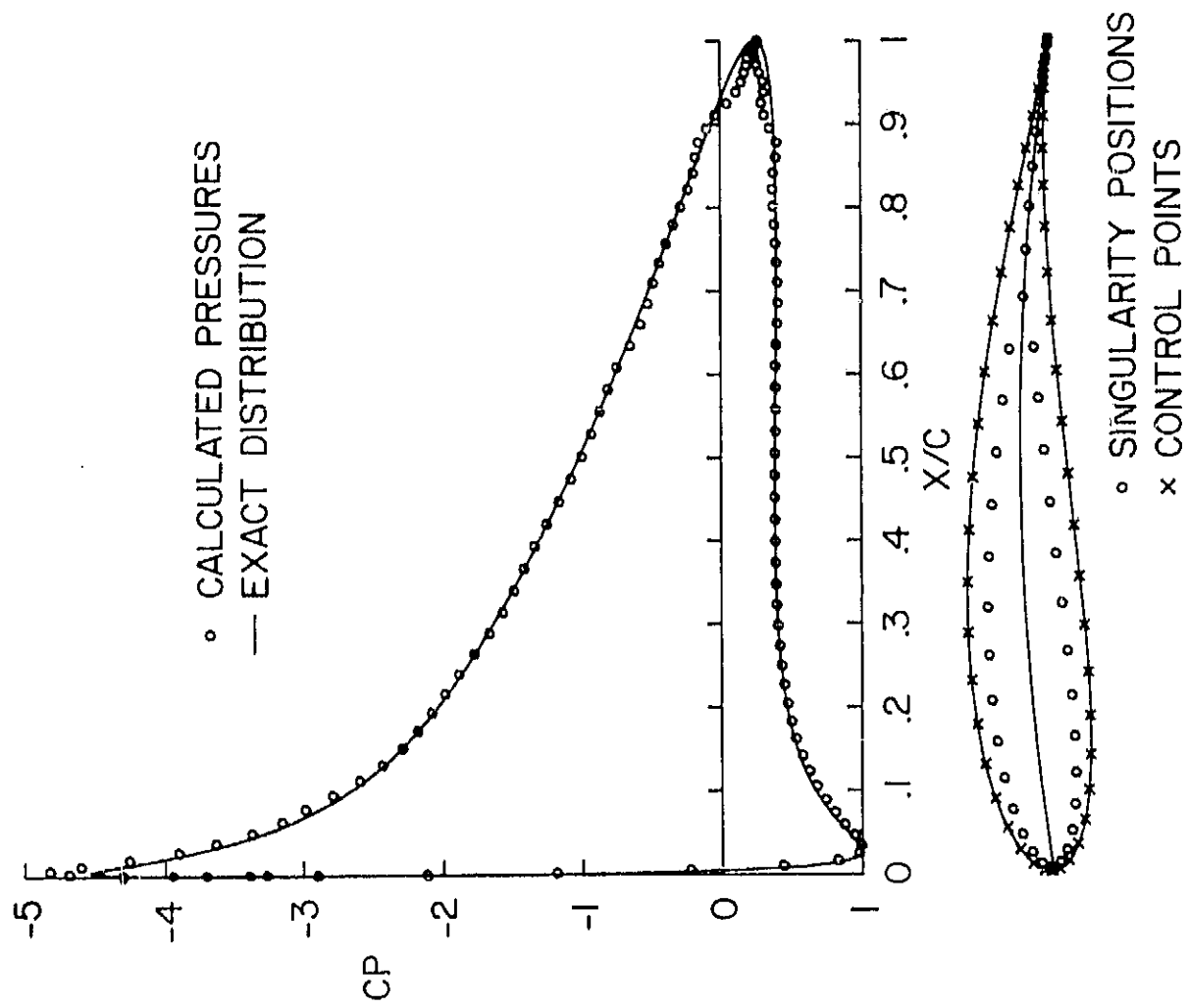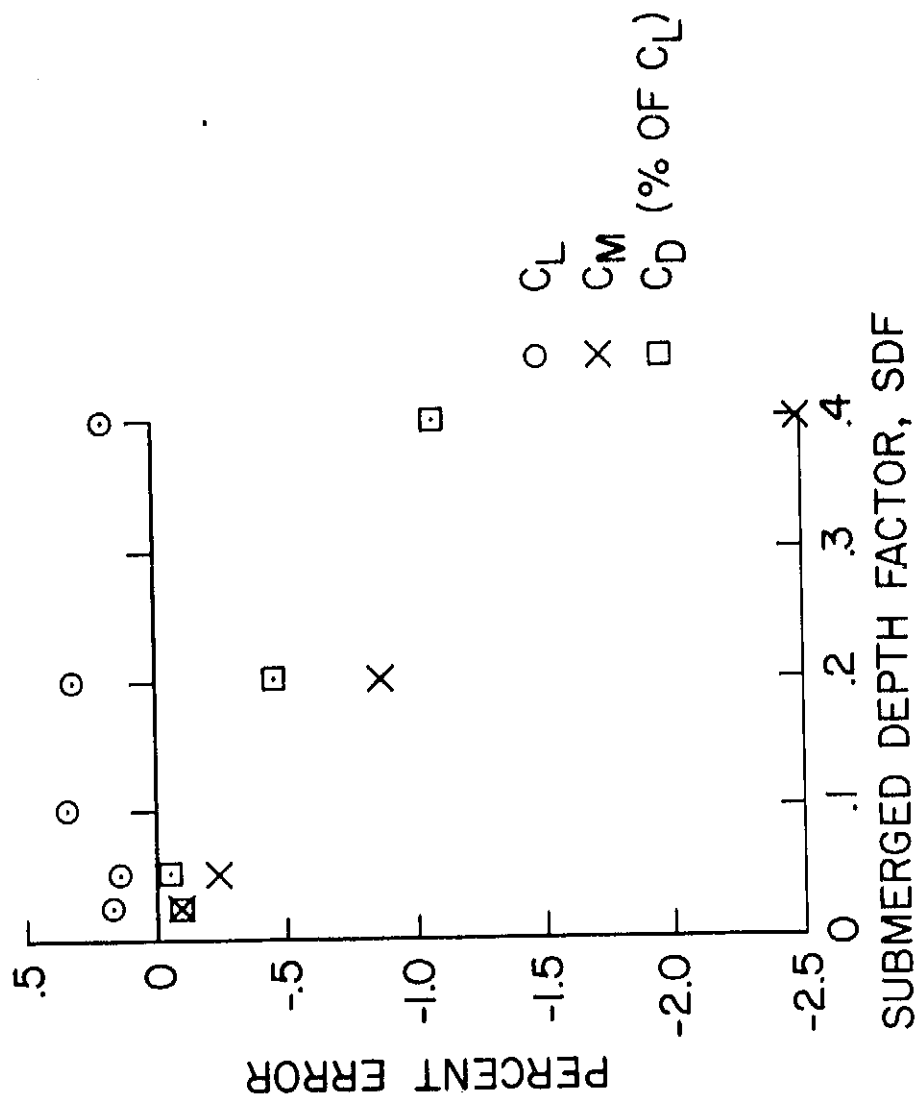
CALCULATED PRESSURES
— EXACT DISTRIBUTION

○ SINGULARITY POSITIONS
× CONTROL POINTS

b) SDF = 0.4.

Fig. 14 Concluded.

Fig. 15 Effect of submerged depth factor, SDF, on the errors in the integrated force and moment coefficients. Basic case as in Fig. 7.
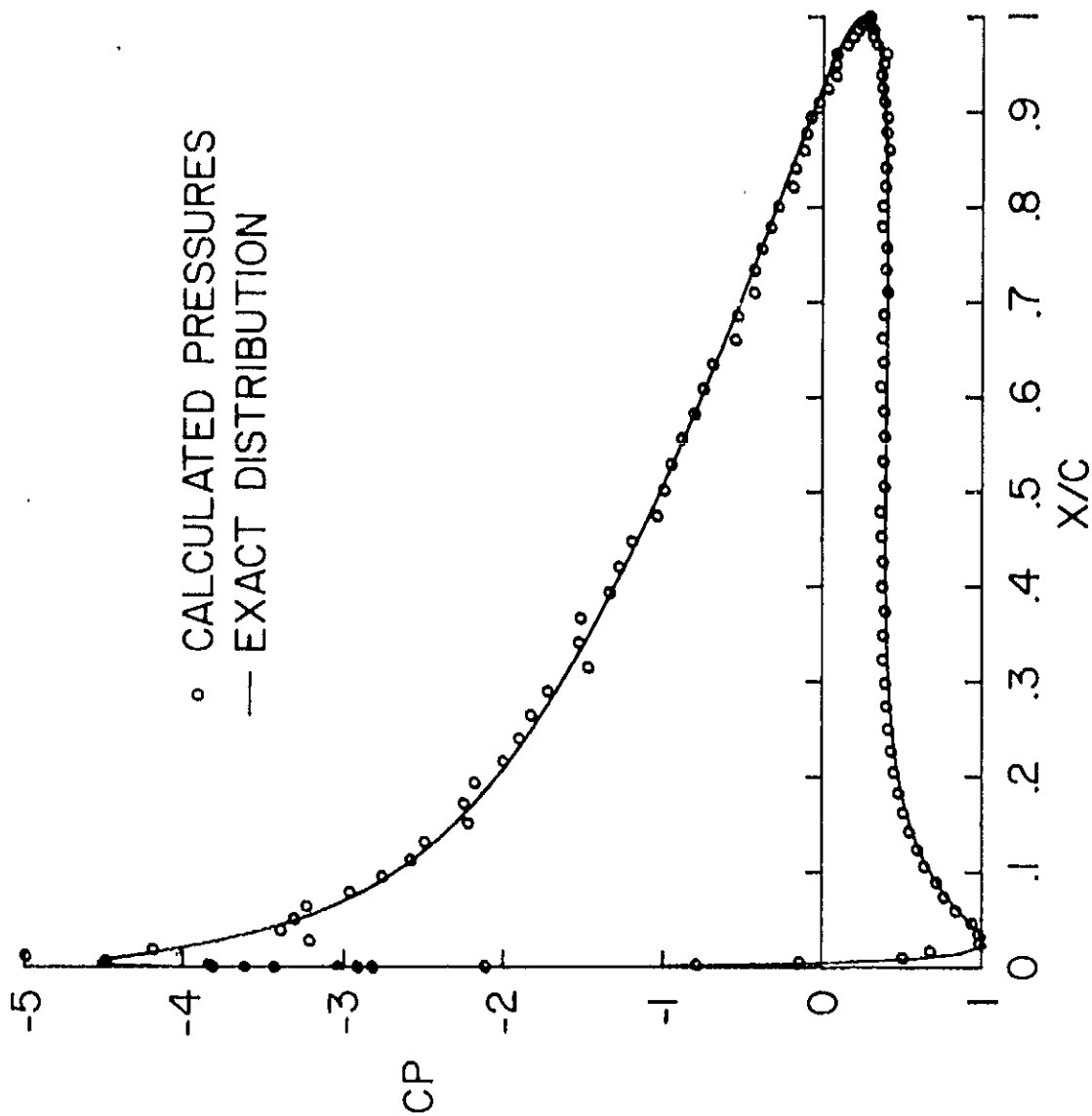
Fig. 16 Pressures calculated at arbitrary points on a Joukowski airfoil at 10° incidence. Model: as in Fig. 7, but with NRF = 1.
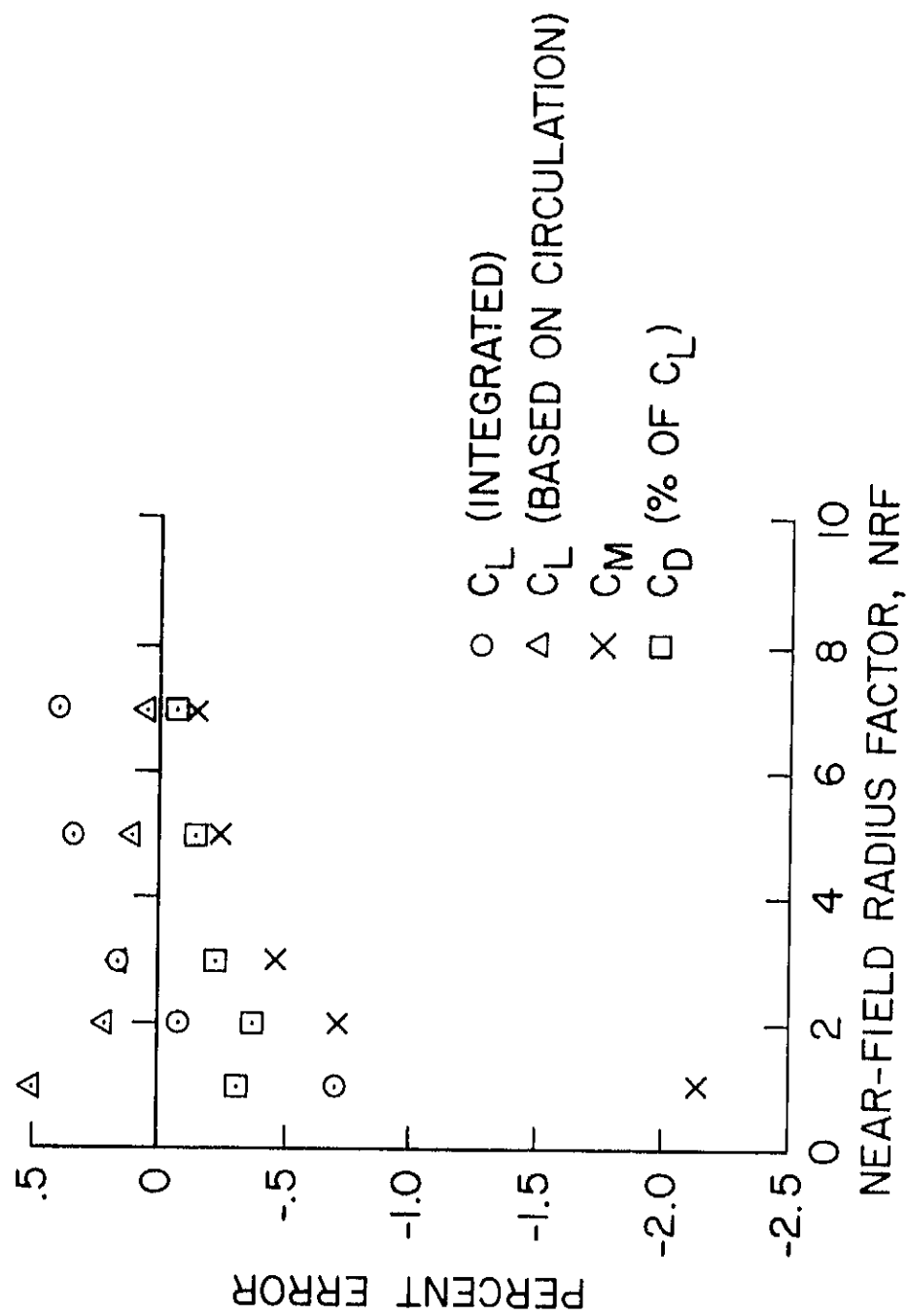
Fig. 17 Effect of near-field radius factor, NRF, on the errors in the integrated force and moment coefficients. Basic case as in Fig. 7.